Water Research 188 (2021) 116532

Contents lists available at ScienceDirect

Water Research

journal homepage: www.elsevier.com/locate/watres

Separation and recovery of ammonium from industrial wastewater containing methanol using copper hexacyanoferrate (CuHCF) electrodes

Rui Gao[a], Luiza Bonin[a], Jose María Carvajal Arroyo[a], Bruce E. Logan[c], Korneel Rabaey[a,b,*]

[a] Center for Microbial Ecology and Technology (CMET), Faculty of Bioscience Engineering, Ghent University, Coupure Links 653, Ghent 9000, Belgium
[b] CAPTURE, Coupure Links 653, Ghent 9000, Belgium
[c] Department of Civil and Environmental Engineering, The Pennsylvania State University, University Park, PA 16802, United States

ARTICLE INFO

Article history:
Received 14 August 2020
Revised 13 October 2020
Accepted 16 October 2020
Available online 17 October 2020

Keywords:
Nitrogen removal
Electrochemical separation
Organics and inorganics separation
Industrial wastewater

ABSTRACT

Ammonium is typically removed from wastewater by converting it to nitrogen gas using microorganisms, precluding its recovery. Copper hexacyanoferrate (CuHCF) is known to reversibly intercalate alkali cations in aqueous electrolytes due to the Prussian Blue crystal structure. We used this property to create a carbon-based intercalation electrode within an electrochemical cell. Depending on the electrode potential, it can recover NH_4^+ from wastewater via insertion/regeneration while leaving organics. In the first phase, different binders were evaluated towards creating a stable electrode matrix, with sodium carboxymethyl cellulose giving the best performance. Subsequently, based on voltammetry, we determined an intercalation potential for NH_4^+ removal of + 0.3 V vs. Ag/AgCl, while the regeneration potential of the electrode was + 1.1 V (vs. Ag/AgCl). Using the CuHCF electrodes 95% of the NH_4^+ in a synthetic wastewater containing 56 mM NH_4^+ and 68 mM methanol was removed with an energy input of 0.34 ± 0.01 Wh g^{-1} NH_4^+. A similar removal of 93% was obtained using an actual industrial wastewater (56 mM NH_4^+, 68 mM methanol, 0.02 mM NO_2^-, 0.05 mM NO_3^-, 0.04 mM SO_4^{2-} and 0.34 mM ethanol), with an energy input of 0.40 ± 0.01 Wh g^{-1} NH_4^+. In both cases, there was negligible removal of organics. The stability of CuHCF electrodes was evaluated either by open circuit potential monitoring (61 h) or by cyclic voltammetry (50 h, 116 cycles). The stability during cycling of the electrode was determined in both synthetic and real streams for 25 h (125 cycles). The charge density (C cm^{-1}) of the CuHCF electrodes declined by 17 % and 19% after 125 cycles in the synthetic stream and the actual wastewater, respectively. This study highlights the possibility of low-cost CuHCF coated electrodes for achieving separation of NH_4^+ from streams containing methanol. The stability of electrodes has been improved but needs to be further enhanced for large-scale applications and long-term operation.

1. Introduction

Industrial sites such as tanneries, urea and fertilizer producers generate waste streams containing ammonium nitrogen (NH_4^+-N). The concentration of ammonium in wastewater generated from the fertilizer industry can range from 6 to 1700 mg L^{-1} (Bhandari et al., 2016). A wide range of established technologies has been investigated to reduce the release of NH_4^+-N into the environment: removal by conversion to nitrogen gas via biological nitrification and denitrification, and recovery via ammonia stripping, ion exchange, membrane technologies or precipitation as struvite. Nevertheless, each of these technologies has high energetic and operational costs, for example 26 to 31 kWh kg^{-1} N using ammonia stripping (Eekert van et al., 2012). Substantial chemical addition is often needed for pH control in stripping and for carbon supplementation during denitrification. Moreover, incomplete separation of ammonium from nitrogen-based fertilizer processing wastewater due to impurities such as methanol and ethanol (Krishnaswamy et al., 2012). The major method for ammonia production is the Haber–Bosch process, which produces more than 96 % of global production of ammonia per year. As this process uses natural gas or oil directly as an energy source, it is one of the largest global energy consumers (14 kWh kg^{-1} N) and greenhouse gas emitters (Qin et al., 2017; Smith et al., 2020). Thus, an effective and economical method is needed to remove and recover ammonium from wastewater. Here we investigated a newly developed strategy using an electrochemical cell (EC) with interca-

* Corresponding author.
E-mail address: Korneel.Rabaey@ugent.be (K. Rabaey).

https://doi.org/10.1016/j.watres.2020.116532
0043-1354/

lation electrodes containing copper hexacyanoferrate (CuHCF) for removing and recovering ammonium from a wastewater containing methanol.

Metal hexacyanoferrate (MHCF) analogues ($A_xM[Fe(CN)_6]_y \bullet zH_2O$) have a well-studied Prussian blue open-framework crystal structure, which have ion insertion properties, and have diverse applications such as peroxide sensors, heavy metals sensors and battery electrodes (Ghica et al., 2013; Mimura et al., 1999; Zhang et al. 2011). Reversible electrochemical insertion of ions into these materials present a valuable alternative to existing nitrogen removal technologies (Wang et al., 2015). MHCF nanoparticles have an open-framework crystal structure containing large interstitial sites (A sites) that allows reversible insertion of cations smaller in ionic radius than the interstitial of the nanoparticles (Pasta et al., 2012). The radii of hydrated Cs^+, Na^+ (3.29 Å), K^+ (3.31 Å) and NH_4^+ (3.31 Å) ions are close to the radii within the complex (3.2 to 4.6 Å) (Klika et al., 2007; Valsala et al., 2009; Wang et al., 2015), making it possible to achieve size-based selective insertion of NH_4^+ (and K^+) (Nightingale, 1959). Among many different MHCFs, the highly crystalline nanoparticles of copper hexacyanoferrate (CuHCF) have been studied for NH_4^+ removal and recovery due to their electrocatalytic ion-exchange capacity, low toxicity and chemical stability in a wide pH range of 0.1 to 10 (Parajuli et al., 2016).

In CuHCF the Cu^{2+} ions are octahedrally coordinated to the nitrogen ends of the CN^- groups, and the Fe^{3+} ions to carbon ends, few K^+ ions probably occupies the "A sites" during nanoparticles synthesis process. On the insertion of NH_4^+ ions, "A" sites are occupied by NH_4^+ ions corresponding to the reduction of some of the carbon-coordinated Fe^{3+} (Supporting information, Figure S1). The carbon-coordinated Fe^{2+} ions are oxidized during regeneration while NH_4^+ ions in the "A" sites are extracted out of the CuHCF. Son et al. (2020) achieved 8.4 ± 1.4 g NH_4^+/ g electrode (cell voltage: +0.3 V) removal capacity of the CuHCF electrodes in a background electrolyte of 10 mM $MgCl_2$ over a range of 10 to 100 mM NH_4Cl. Kim et al. (2018b) used CuHCF based electrodes to remove NH_4^+ from domestic wastewater (5 or 3.4 mmol L^{-1}) and obtained a maximum NH_4^+ removal efficiency of 85 % with high selectivity over Na^+ under a constant cell voltage over 200 s. However, the performance of electrodes with industrial wastewaters and the effects of potentials on insertion/regeneration were not examined. Moreover, the many previously reported tests only reported the stability over hours, whereas in practice, an electrode will need to be stable over many months to years.

The goal of this study was to evaluate the performance and stability of CuHCF based electrodes under fixed potentials for insertion/regeneration of NH_4^+ from a specific industrial wastewater containing methanol. We initially assessed the suitability of two binders for the assembly of CuHCF electrodes and studied the impact of potentials on the removal efficiency of NH_4^+ from a synthetic stream in order to establish the potential window. NH_4^+ removal tests were then performed with both synthetic and actual industrial streams after establishing an optimal binder and working potentials. The stability and cycling life of the electrodes were examined through the evolution of the current density and the dissolution of the functional coating material over time.

2. Materials and methods

2.1. Synthesis of CuHCF and electrode preparation

CuHCF powder was synthesized through co-precipitation (Wessells et al., 2011). Equal volumes of 0.1 M $Cu(NO_3)_2$ (Sigma-Aldrich, 99-100 %) and 0.05 M $K_3[Fe(CN)_6]$ (Sigma-Aldrich, 99%) were simultaneously added at a flow rate of 0.5 mL min^{-1} to deionized water. Ultrasound (BANDELIN, HF-Frequency 35 kHz, Germany) was applied to reduce aggregation and to obtain a homogenous precipitate. The precipitates were centrifuged at 14560 × g for 15 min, and the residue obtained was washed several times with deionized water for washing out unreacted ions. The final product was dried in a 105°C oven for 5 h to obtain a CuHCF powder. The dried CuHCF powder was ground into a uniform powder with a ceramic mortar and pestle and then a granulometric separation was performed using a 50 µm pore size stainless steel sieve (Fisher Scientific, Belgium).

To make CuHCF electrodes, a slurry of 80% wt./wt. CuHCF powder (72.8 mg per electrode) as conductive material, 15% wt./wt. carbon black as conducting additive (Vulcan XC72R, Cabot) and a 5% wt./wt. binding agent was mixed with 400 µL of deionized water. The electrode slurry was mixed with a ceramic mortar and a pestle. A graphite carbon plate with a projected surface area of 10 cm^2 and a thickness of 0.25 cm was used as the substrate material. The substrate was polished on sandpaper and thoroughly rinsed with ethanol and deionized water before loading the CuHCF slurry using a flat scraper. Three layers in total were manually spread with a spatula on the pre-treated surface of graphite carbon, and each layer was dried 45 min at 105°C. A stainless-steel foil was cut in 2 × 5 cm^2 (projected surface area = 10 cm^2, thickness = 0.2 mm; SS304, GOODFELLOW, England) was used as current collector and glued to the non-treated surface of graphite carbon plate by silver paint. Finally, the four lateral sides of the electrodes (comprising the silver painted surfaces) were insulated with epoxy glue (TS10, THORLABS, Europe). New electrodes were rinsed with Milli-Q water before applying in tests, and a new electrode was used in each removal test.

2.2. Screening of binding agents

Carboxymethylcellulose sodium salt (CMC) (Sigma-Aldrich, 99.99%, Germany) and poly(3,4-ethylenedioxythiophene)-poly(styrenesulfonate) (PEDOT:PSS) (Sigma-Aldrich, 97%, Germany) are able to enhance ionic and electronic conductivity of the electrode, which were examined as binding agents. Three tested slurry compositions (slurry A, B and C) containing one of the two binding agents (Supporting information, Table S1) were used to evaluate the impact of binders on the performance of CuHCF electrode by cyclic voltammetry (CV). Electrodes coated with one of the three different CuHCF slurry compositions were firstly weighed to unify weights before analyses. Then, the electrodes were rinsed with Milli-Q water and separately moved into a 3-electrode setup (60 mL open glass beakers) filled with 1 mol L^{-1} of NH_4Cl for performing CV analysis at 1 mV s^{-1} under 24°C. The counter electrodes were graphite rods and the references Ag/AgCl (3 M KCl, +0.197 V vs a standard hydrogen electrode (SHE), Bio-Logic Science Instruments SAS, Claix, France). After completing 10 cycles of CV program for each electrode, CuHCF electrodes were separately immersing into a setup containing fresh electrolyte (1 mol L^{-1} of NH_4Cl) accompanied by constant stirring over 72 h. Then electrodes were moved back to the electrochemical setup for another 10 cycles of CV analyses to evaluate the effect of binding agents on the stability of the CuHCF electrode over long-term immersion.

2.3. Ammonium removal tests

Ammonium removal tests were performed in a custom-built electrochemical cell (EC) (Fig. 1). The EC consisted of two compartments (internal dimensions: 2 × 5 × 0.25 cm) made from two Perspex® frames separated by an anion exchange membrane (AEM) (Ultrex AMI-7001, Membranes International Inc., USA). A graphite carbon electrode without CuHCF coating was used as counter electrode (dimensions: 2 × 5 × 0.25 cm). The CuHCF working elec-

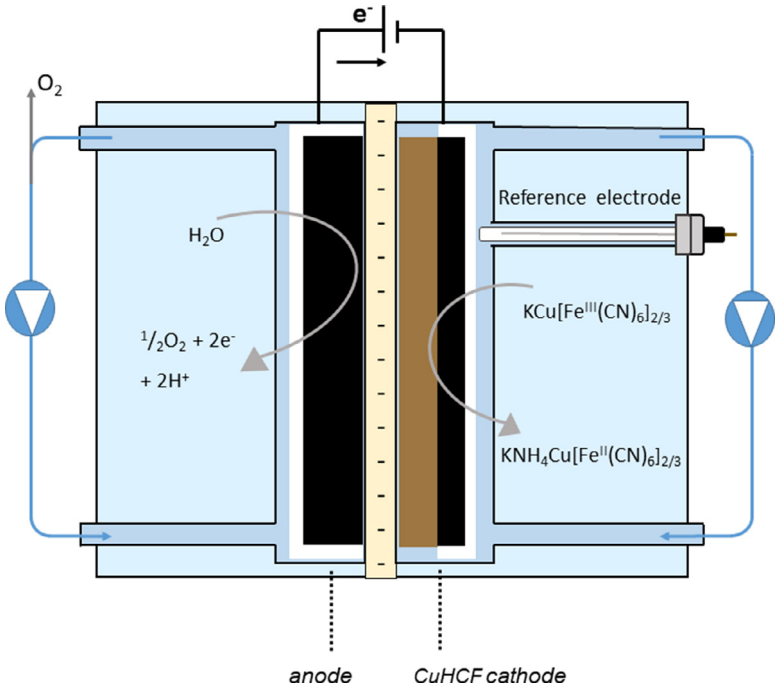

Fig. 1. Overview of the system for separation of NH4+ from the wastewater containing methanol with CuHCF electrode.

Table 1
pH, conductivity and the composition of synthetic and real stream.

Species	Synthetic stream (mg L^{-1})	Real stream (mg L^{-1})
pH	6.15	7.05
Conductivity (mS cm^{-1})	4.72	4.9
NH_4^+(mg L^{-1})	1008	1007.7
CH_3OH (mg L^{-1})	2000	2131.8
C_2H_6O (mg L^{-1})	–	27
NO_2^- (mg L^{-1})	–	< 0.3
NO_3^- (mg L^{-1})	1008	5.5
SO_4^{2-} (mg L^{-1})	–	4.6
Al (mg L^{-1})	–	0.1
Na (mg L^{-1}) Cr (mg L^{-1}) Zn (mg L^{-1}) Fe (mg L^{-1})	–	<0.1

trode (slurry C) and counter electrode were inlaid in the anode and cathode compartment, respectively. Rubber sheet seals were sandwiched between compartments and AEM to create a liquid-tight seal, and the frames were bolted together. A VSP Multi Potentiostat (Bio-Logic Science Instruments SAS, Claix, France) was used for electrochemical control. The half-cell potential of the working electrode was determined with a Ag/AgCl reference electrode (assumed as +0.197 V vs SHE) in the compartment of CuHCF electrode.

The appropriate insertion and regeneration potentials were evaluated by performing NH_4^+ removal tests using the synthetic stream (Table 1) under constant insertion potentials of 0.2, 0.3, 0.4, 0.5 and 0.6 V, and regeneration potentials of 0.9, 1.0 and 1.1 V vs. Ag/AgCl. The operational time for each potential was defined as the time needed for the absolute current to reach a steady state. Both anode and cathode compartments were first fed with synthetic wastewater and then recirculated at a flow rate of 8 mL min^{-1} with a peristaltic pump (Watson Marlow 530U, USA). The total volume of the recirculated solution that filled the flow cell and tubing was 40 mL in terms of recirculation rate of 20 mL min^{-1} (HRT of 2 min) for each compartment. The same electrode was applied in insertion or regeneration tests to prevent differences due to possible inconsistencies in the preparation of the coating material. The charge densities and the NH_4^+ concentrations were recorded and analyzed to investigate the appropriate insertion and regeneration potentials.

Longer ammonium removal tests, which included 20 cycles of alternating insertion and regeneration processes, were run with synthetic and industrial wastewater at the selected insertion and regeneration potentials of 0.3 and 1.1V vs. Ag/AgCl. Electrochemical cell with same configuration as previous tests was applied in long-term ammonium removal experiments. The real wastewater (Table 1) was collected from the effluent of a chemical company producing nitrogen fertilizer and nitrogen-based chemicals. The wastewater was filtered through a 0.22 μm pore size filter (type GVWP, MilliporeSigma) before use. The working electrode was regenerated before the beginning of the tests by applying a potential of 1.1 V vs Ag/AgCl until the current reached a steady state. A fresh synthetic stream was applied in each regeneration cycle, but the same synthetic or real stream was maintained during the 20 cycles of insertion process. The concentration of NH_4^+ was evaluated to determine the capacity of insertion and regeneration for each cycle.

2.4. Stability and long-term cycling of CuHCF electrode

The stability of the CuHCF electrode was assessed with a 3-electrode system in a beaker containing 60 mL electrolyte. A graphite rod (Dimensions: 0.03 cm^2 x 6 cm) (National electrical carbon BV, Netherlands) was used as counter electrode. The electrolyte containing 1 mol L^{-1} NH_4NO_3 or NH_4Cl was used to evalu-

ate the stability of the CuHCF based electrode through open circuit potential (OCP) and CV analyses. The OCP analysis was performed in a three-electrode setup (60 mL glass beaker) with continuous stirring, and the CVs were performed at a scan rate of 1 mV s^{-1} in a suitable medium. The stability of electrodes was evaluated via OCP and CV by observing the changes in the current density and CuHCF particles physically peeling off in the electrolyte.

The long-term cycling performance of CuHCF based electrodes over more than 100 insertion and regeneration cycles was performed in a flow cell using either synthetic or actual wastewaters using only a single insertion and regeneration potential (0.3 and 1.1 V Ag/AgCl). Samples for Cu^{2+} analysis were taken regularly, centrifuged at 14650 xg for 5 min, filtered through a 0.22 μm pore diameter syringe filter (type GVWP, Millipore-Sigma), and acidified with nitric acid (10%) before storage and later analysis.

2.5. Analytical methods

XRD measurements of CuHCF particles were carried out on a Bruker D8 Discover XRD system equipped with a Cu X-ray source (λ = 1.5406 Å) and a linear X-ray detector using a Si sample cup. Ex-situ XRD measurements were carried out in air at atmospheric pressure at 24°C. Scanning electron microscopy (SEM) images of CuHCF particles were recorded at an acceleration voltage of 15 keV with a JSM-7600F field emission SEM instrument (Phenom ProX, Thermo fisher scientific, USA). Samples were mounted on aluminum stubs using a double-sided adhesive carbon tape and sputtered with Au to reduce charging effects. The particle size of CuHCF after filtration with 50 µm stainless steel sieve was determined by light microscopy with a camera and semi-automatic image analysis software (Olympus, Japan). Dissolved copper from long-term cycling tests was measured by flame-atomic adsorption spectrometry (AAS) (Shimadzu AA-6300, Shimadzu Scientific Instruments, Somerset, NJ, USA). Prior to analysis, samples were filtered with 0.02 µm and acidified with 10 % nitric acid. The concentration of NH_4^+ was determined in a Metrohm 761 compact ion chromatography system (Metrohm AG, Herisau, Switzerland). Separation occurred at 15°C in a Metrosep C6-150/4 column, equipped with a Metrosep guard column/4.0. Methanol was executed using a gas chromatography system consisting of a AOC-20 autosampler (Shimadzu, Japan) and Rtx-624 GC Capillary Column (0.18mm x 1.00µm x 30m). Anions from real stream were determined in a 930 compact ion chromatography system (Metrohm AG, Herisau, Switzerland) with chemical suppression and conductivity detector. Separation occurred at 15°C in a Metrosep A Supp 5-150/4 column, equipped with a Metrosep A Supp 4/5 guard column/4.0.

3. Results and discussion

3.1. Copper hexacyanoferrate synthesis and binder selection

The CuHCF powder had a highly crystalline structure that consisted of aggregates of nanoparticles with sizes ranging from 20-50 nm (Fig. 2a,b). The determined composition based on X-ray diffraction (Fig. 2a) was $K_{0.76}$ $Cu[Fe(CN)_6]_{0.66}$. The size of most of CuHCF nanoparticles was below 50 µm after the granulometric separation, but complete dispersion of the NPs could not be achieved as CuHCF nanoparticles coalesced as large agglomerates under the conditions of preparation of the adsorbent (Supporting information, Fig. S1).

CV analysis (3-electrode system) of three electrode slurries created with different binders resulted in similar mid-point potentials of 0.79 ± 0.03 V (vs. Ag/AgCl) before the immersion test, indicating no impact of the type of binders on the oxidation or reduction

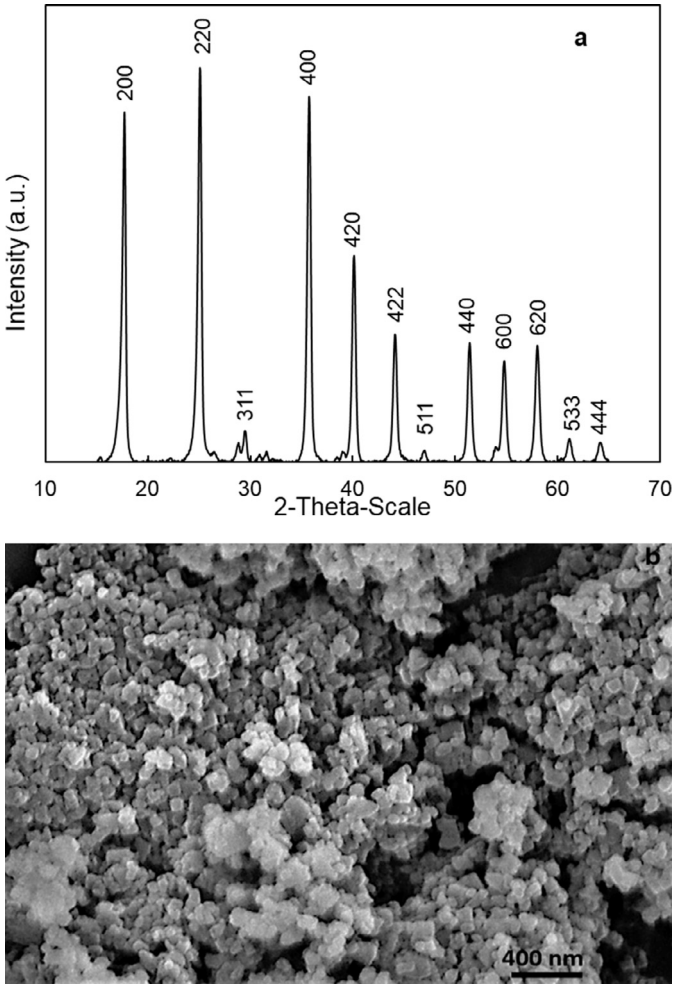

Fig. 2. (a) X-ray diffraction patterns of CuHCF showing a highly crystalline material. (b) SEM of CuHCF indicating a crystal size of 20–50 nm (Scale bar, 400 nm).

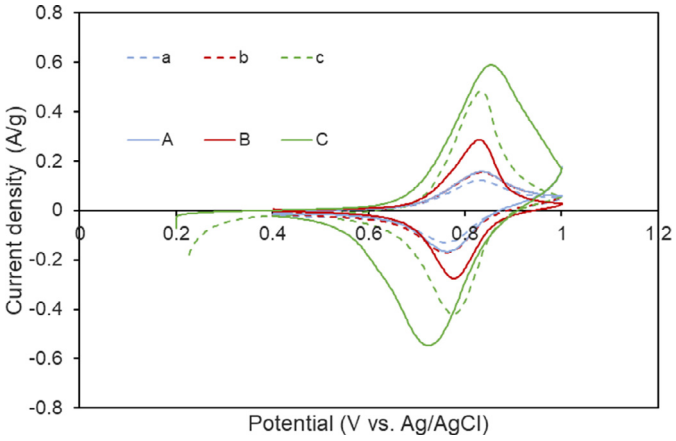

Fig. 3. Cyclic voltammetry (CV) analysis of CuHCF with different binders. A and a: PEDOT:PSS and carbon black, B and b: PEDOT:PSS, C and c: CMC and carbon black. Solid lines: before immersion test, and dashed lines: after a 3-day immersion test.

reactions (Fig. 3). The ratio between the anodic and cathodic peak current density was close to 1 for all electrodes, consistent with a reversible electrochemical reaction (Kim et al., 2018a). Slurry C (CMC and carbon black) had the highest redox peak current densities of 0.58 and -0.54 A g $CuHCF^{-1}$. The conductivity of slurry C was in between that of slurry A and B, which indicated that the high current density of slurry C was most likely the result of a

more efficient interaction of the CuHCF with the NH_4^+ ions rather than an increased material conductivity (Supporting information, Table S2).

After 72 h of immersion in 60 ml glass beakers, the electrolytes in tests with slurry A and C remained clear, and no particles were observed in the solution at pH 6.15. The impact of carbon black on electrode stability was further investigated by comparing CV analysis of slurry B with other two slurries. The oxidation (regeneration) peak of the electrode with slurry B decreased from 0.35 to 0.18 A g $CuHCF^{-1}$ while the reduction (insertion) peak current density declined from -0.35 to -0.2 A g $CuHCF^{-1}$, which were all lower than other two slurries (Fig. 3). The electrolyte in the experiment with slurry B turned brownish after immersion indicating degradation of the electrode. Although PEDOT:PSS and CMC can be independently used as sole binders (Li et al., 2017; Wang et al., 2012), carbon black is still needed to ensure a close electrical connection between CuHCF material and binders as well as to stabilize the electrochemical performance of the electrodes (Shi et al., 2017). The redox peak current densities of slurry C remained considerably higher compared with the other two slurries (Fig. 3), indicating a more stable performance of the CMC binder than the PEDOT:PSS. Therefore, the CMC binder (slurry C) was selected for further experiments.

3.2. Ammonium removal from synthetic and industrial wastewater

The optimal NH_4^+ insertion and electrode-regeneration potentials for ammonia removal were selected based on four parameters: the charge density (C cm^{-2}) (Supporting information, Fig.S5), the concentration of inserted/extracted NH_4^+ (mg L^{-1}), the energy input (Wh g^{-1} NH_4^+) (Supporting information, Eq.1) and the insertion/regeneration capacity (mg NH_4^+ g $CuHCF^{-1}$). The effect of the insertion/regeneration potential on the insertion/desertion of NH_4^+ was investigated with a constant potential (from 0.2 to 1.1 V vs. Ag/AgCl). The highest insertion capacity of 70 mg NH_4^+ g $CuHCF^{-1}$ and associated lowest energy input of 0.11 Wh g^{-1} NH_4^+ were achieved at 0.3 V vs. Ag/AgCl (Supporting information, Table S3), therefore this potential was selected for further tests. For regeneration, 1.1 V vs. Ag/AgCl was chosen since it resulted in the highest concentration of released NH_4^+ and had lowest energy input among all the tested regeneration potentials (Supporting information, Table S4).

The highest removal rate of NH_4^+ was obtained through 20 cycles of ammonium removal tests, but the insertion capacity of electrodes declined steadily over time. In the first 10 insertion cycles (pH 6.15), 772 ± 1 mg L^{-1} NH_4^+ was removed from a total NH_4^+ concentration of 1008 mg L^{-1} at an energy input of 0.34 ± 0.01 Wh g^{-1} NH_4^+ (Fig. 4a,c), which indicated a removal rate of 715 ± 1.22 mg NH_4^+ L^{-1} h^{-1} corresponding to 17.16 ± 0.03 g NH_4^+ L^{-1} d^{-1}, with a removal capacity of 40 ± 1.12 mg NH_4^+ g $CuHCF^{-1}$ per cycle. The removal rate after 10 cycles was higher than conventional NH_4^+ removal rates such as nitrification/denitrification (33 mg NH_4 L^{-1} h^{-1}) and NH_4^+ stripping (42 mg NH_4 L^{-1} h^{-1}) from streams containing more than 1000 mg L^{-1} of ammonia (Sharma and Sanghi, 2012; Zöllig et al., 2017), which suggested the material could be useful for NH_4^+ removal/recovery if maintained at this level. However, over the next 10 cycles, the insertion capacity declined sharply to only 0.01 g NH_4^+ g $CuHCF^{-1}$ by the final cycle, with a removal rate of 166 ± 0.17 mg NH_4 L^{-1} h^{-1} and a cumulative 957 ± 0.12 mg NH_4^+ L^{-1} ammonium removed from the synthetic stream (1008 mg NH_4^+ L^{-1}).

The decrease in NH_4^+ removal capacity of the electrode over successive cycles could have occurred for at least three different reasons: degradation of CuHCF material, incomplete regeneration, and decreasing NH_4^+ concentrations. First, the electrochemical activity of CuHCF lost over time due to the degradation of CuHCF

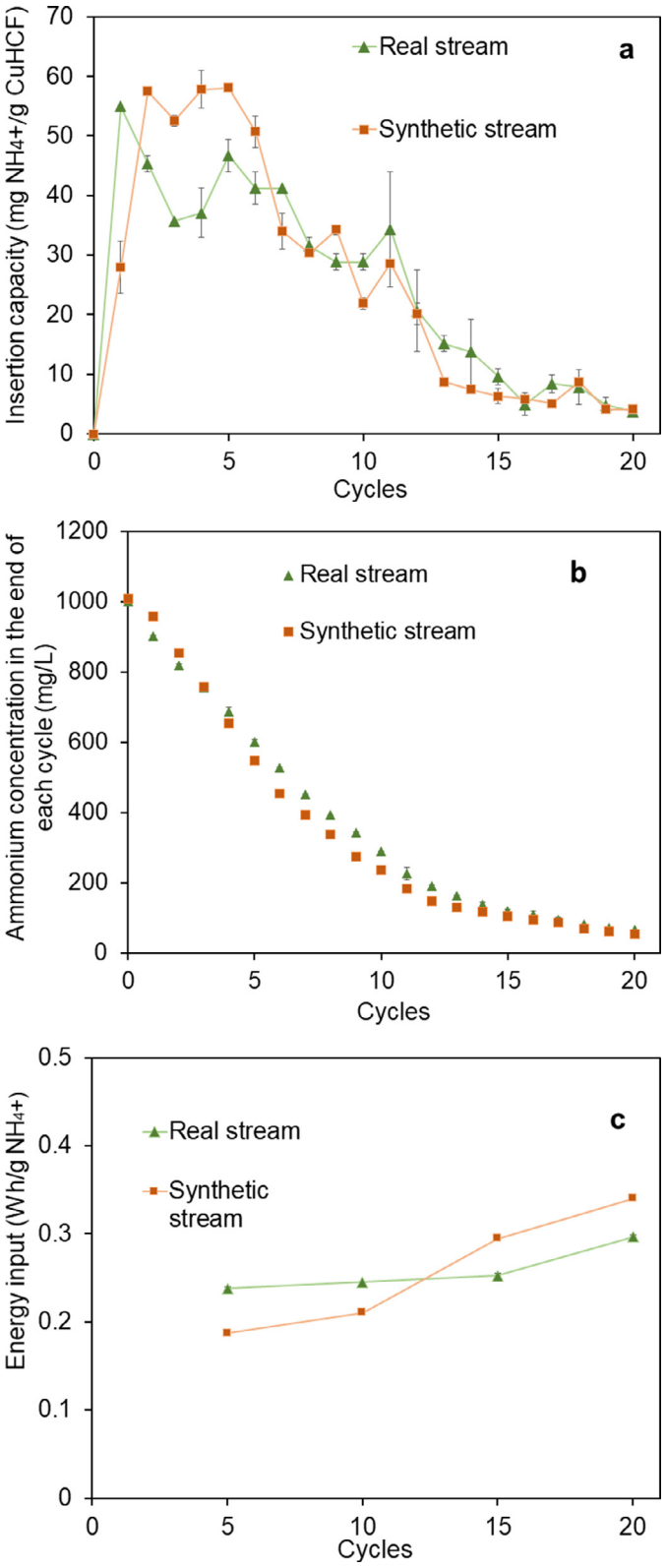

Fig. 4. (a) Insertion capacity of the electrode from a synthetic and real stream, (b) Concentration of inserted NH4+ during NH4+ removal from the synthetic and real stream, and (c) Comparison of energy input after 5,10,15 and 20 insertion cycles with the synthetic and real stream.

should play the dominant role in the declined removal capacity. In addition, the adsorption kinetics of CuHCF was unusual in that there was an appreciable decline of capacity after reaching a pseudomaximum (Parajuli, 2016), probably due to the degradation of CuHCF material released K^+ and introduced through competition by K^+ ions during cycling. Second, the incomplete regeneration of the electrode between cycles could have contributed to a declined capacity of the electrode. The extraction efficiency over the first 5 regeneration cycles averaged 80.1 ± 0.4 %, calculated based on the amount of NH_4^+ that remained in the electrode from the previous insertion, and it rose slightly to 88.9 ± 0.4 % after 20 cycles. Nevertheless, the insertion capacity decreased by 65 % between the first and the last cycle of the experiment (Fig, 4). Thus, ~10 % of the inserted NH_4^+ remained in the CuHCF electrode after regeneration. XRD analysis of CuHCF particles after 20 cycles showed that the crystal framework of CuHCF particles was stable, but the peak at 2θ of 17.8 after cycling was higher than in the original particles (Supporting information, Fig S2). This peak area can be attributed to a partial replacement of K^+ ions by NH_4^+ ions (Parajuli, 2016), which would result in a declined insertion capacity. Third, the initial liquid NH_4^+ concentration in each cycle probably affected the observed insertion capacity. This was investigated in a separate test with a new CuHCF electrode in a synthetic stream containing a lower initial NH_4^+ concentration of 30 mmol L^{-1} (540 mg L^{-1}). After 10 cycles, the insertion capacity of the electrode was 0.089 g NH_4 g $CuHCF^{-1}$, which was similar to the insertion capacity of 0.091 g NH_4 g $CuHCF^{-1}$ measured in an electrolyte with 30 mmol L^{-1} (Supporting information, Fig S4). Jiang et al. (2018) indicated that the concentration of removed NH_4^+ declined when the liquid NH_4^+ concentration was below 10 mmol L^{-1}. Nonetheless, Son et al. (2020) reported that the insertion capacity maintained constant over a range of 10 to 100 mmol L^{-1} of NH_4^+. Therefore, the insertion capacity of electrodes is likely only affected when the initial concentration of NH_4^+ in the liquid is lower than 10 mmol L^{-1}.

The energy input needed for the regeneration process grew steadily over 20 cycles. The energy input of regeneration in the first 5 cycles was 1.21 ± 0.01 Wh g^{-1} NH_4^+ (Supporting information, Table S5), compared to 2.53 ± 0.01 Wh g^{-1} NH_4^+ after 20 cycles. The energy input of insertion also increased from 0.19 ± 0.01 Wh g^{-1} NH_4^+ in the first 5 cycles, compared to 0.34 ± 0.01 Wh g^{-1} NH_4^+ at the end (Fig, 4c). Therefore, the energy input of NH_4^+ recovery in the first 5 cycles was combined 1.40 ± 0.01 Wh g^{-1} NH_4^+ in total, and then it grew to 2.87 ± 0.01Wh kg^{-1} NH_4^+ after 20 cycles. The regeneration process resulted in higher energy input for NH_4^+ recovery, indicating the lattice distortion of CuHCF over multiple cycles led to higher energy needs to push the inserted NH_4^+ back out of the material.

The NH_4^+ removal from a real wastewater (Fig, 4b, c) was similar to that obtained for the synthetic wastewater. After 20 insertion cycles on the real stream (pH 7.02), 936.5 ± 0.5 mg NH_4^+ L^{-1} were removed out of the initial 1008 ± 0. mg L^{-1} at an energy input of 0.40 ± 0.01Wh g^{-1} NH_4^+. The removal rate over 20 cycles was 425.7 ± 0.3 mg NH_4^+ L^{-1} h^{-1} corresponding to 10.2 ± 0.1 g NH_4^+ L^{-1} d^{-1}, with a removal capacity of 31.8 ± 1.1 mg NH_4^+ g $CuHCF^{-1}$ per cycle. As we had observed when using synthetic wastewater, the electrode could not be completely regenerated after each cycle. The regeneration efficiency of the electrode rose slightly from 87.82 ± 0.55 % in the first 5 cycles to 89.19 ± 0.19 % after 20 cycles (Table S6). The energy input of the first 5 regeneration cycles was 1.3 ± 0.1 Wh g^{-1} NH_4^+ and increased gradually to 2.5 ± 0.1 Wh g^{-1} NH_4^+ at the end. The energy input needed for insertion and regeneration was 2.8 ± 0.2 Wh g^{-1} NH_4^+ in total. This indicated that the matrix in the real stream did not noticeably affect the performance of the electrode since both tests with synthetic and real stream revealed similar trends over the cycles (Fig. 4). Additionally, the concentration of anions and organics in the real stream was not affected by the insertion/regeneration process (Supporting information, Table S7) .

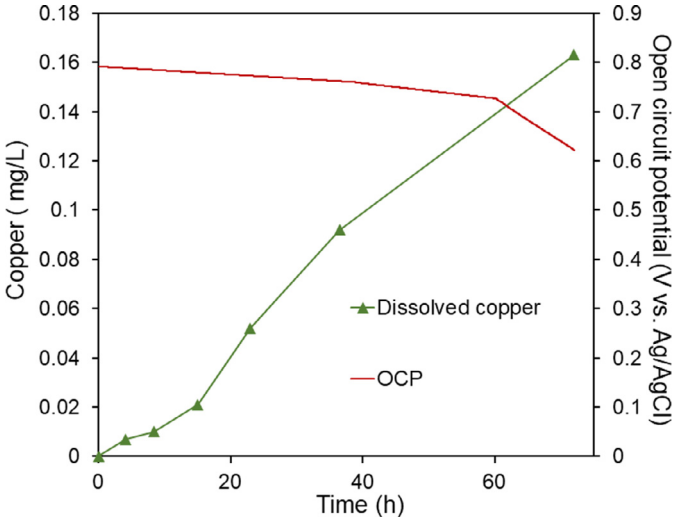

Fig. 5. Open circuit potential of the CuHCF electrode in 1 M NH4NO3 over 72 h.

3.3. Stability and long-term cycling test of CuHCF electrode

As the anions in solution might react with the electrode and affect its stability, the effect of chloride and nitrate containing electrolytes was examined in CV cycling tests over 62 h in 3- electrode system (Supporting information, Fig. S8a). The anodic peak potentials (E_{pa}) from NH_4Cl and NH_4NO_3 were very similar (0.83 and 0.85 V vs. Ag/AgCl, respectively) and the cathodic peak potentials (E_{pc}) from the two supporting electrolytes were comparable as well, with 0.77 V for NH_4Cl and 0.74 V vs. Ag/AgCl for NH_4NO_3. The mid-point potential ($E_{1/2}$) of NH_4NO_3 was 0.79 V vs. Ag/AgCl after 10 h of analysis, which was only 0.01 V lower than the $E_{1/2}$ at the onset, indicating a reversible process after 10 h. However, there was no peak observed after 10 h of CV analysis in NH_4Cl, and accompanied by a noticeable odor. The conductive material completely disintegrated after rinsing with distilled water probably due to Cl_2 produced by the oxidation at the carbon anode under the high counter potential (Supporting information, Fig. S9).

NH_4NO_3 was selected as supporting electrolyte to investigate the stability of CuHCF electrode over time to avoid possible damage to it by chlorine generation. First, the open circuit potential (OCP) over time was examined during immersion of the electrode in a 1 M NH_4NO_3 electrolyte (3-electrode system, 60 ml glass beaker). The OCP showed a slight decrease during the first 60 h, with a more significant reduction after 61 h (Fig. 5). The dissolution of the electrode was reflected in the change in the color of the electrolyte from clear to light brown. After 61 h, fine particles were visible in the solution and on the bottom of the flask (Supporting information, Fig. S6a, b). Analysis of the composition of the electrolyte revealed copper in solution, showing electrical current was not essential to cause damage to the electrode. Released K^+ was observed after the OCP analysis of the CuHCF electrode over 50 h indicating binder degradation during the long-term tests (Supporting information, Fig.S7). Further structural modification of CuHCF electrodes and an optimal binder are needed to be investigated to improve stability.

The stability of the CuHCF electrode was further evaluated in a CV analysis with 1 mmol L^{-1} of NH_4NO_3 during 62 hours in 3-

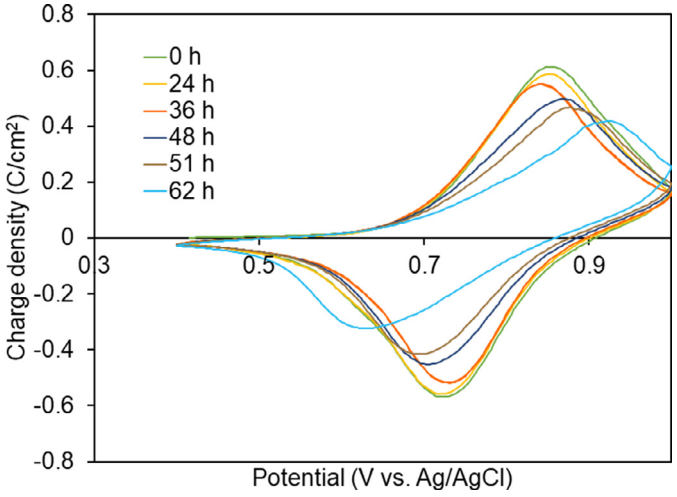

Fig. 6. CVA stability test of CuHCF electrode in 1M NH4NO3 over 62.2h at room temperature

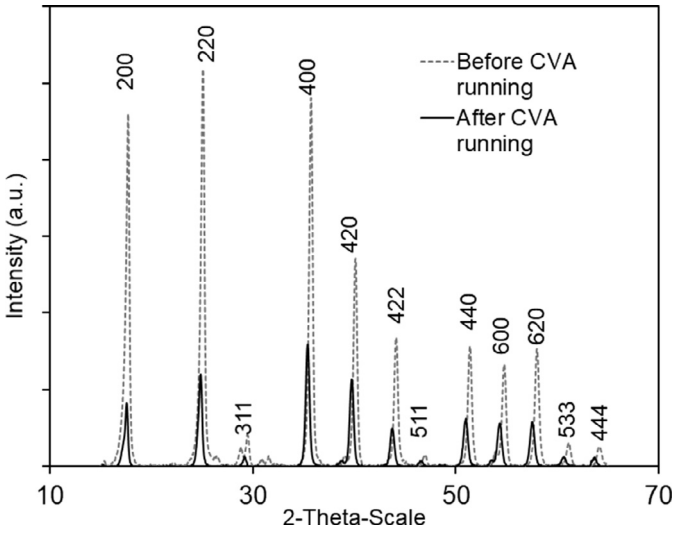

Fig. 7. XRD analysis of mixture of CuHF, black carbon and CMC before CVA stability test (dashed line) and after CVA satability test (solid line).

electrode system (Fig. 6). A sequence of CVs contained repeated insertion and regeneration cycles was performed. During this time, the anodic and cathodic potentials peaks slightly shifted to more positive and negative potentials at 48 h, respectively, then further distanced until 51 h, at which time pieces of the conductive material peeled off of the electrode. Finally, the CV after 62 h showed anodic and cathodic current peaks at 0.63 and 0.93 V vs. Ag/AgCl, respectively. Two phenomena were probably responsible for the shift in the redox potentials in this system: insufficient regeneration that could limit the adsorption sites; and physical and/or chemical separation of the catalyst from the conductive support. During the ammonium removal test on both the synthetic and real stream, part of the active sites on the electrode surface was occupied by the inserted NH_4^+ after regeneration. Therefore, the limiting amount of electroactive spots on the surface lead to a shift in the CV towards more anodic/cathodic potentials (Champagne and Kirtman, 2001). At the same time, detachment of the material was observed after 51 h, indicating that the CuHCF material lost physical contact with the electrode substrate due to the lattice distortion (Fig. 7). XRD comparison of a new CuHCF electrode with the electrode after long-term CV analysis, showed no evident change from the position of three main peaks (at 2 θ = 17.8°, 25° and 35°), demonstrating that the crystal structure of the CuHCF on the electrode could be maintained upon the insertion/regeneration process. However, the peak height of those three main peaks decreased dramatically, and peaks broadening after long-term CV analysis indicated a lattice distortion of the CuHCF structure caused by residual stress during insertion and regeneration (Pasta et al., 2016; Pothanamkandathil et al., 2020; Yeh et al., 2007). Wang et al. (2020) indicated the transformable structure of CuHCF particles during cycling, which can be considered as a distortion of the internal atoms. Thus, an unaccommodated binding material and morphology controlling method were needed for improving CuHCF structure.

The long-term cycling behavior of CuHCF electrodes under appropriate potentials was evaluated with synthetic and real industrial streams (Supporting information, Fig.S10). After 115 cycles (6.12), the charge density from the synthetic stream dropped by 17 %, compared to 19 % for the real stream. The target operational time was 50 h. However, dissolved copper from the coating was measured and coating particles peeled off from the electrode after 24 h as well (Supporting information, Fig.S12). In the synthetic stream, only 0.009 mg L^{-1} Cu^{2+} was detected after 6 h (Supporting information, Fig.S11). The concentration of dissolved copper increased up to 0.417 mg L^{-1} after 25 h. Also, in the real stream, copper were measured in the solution after 6 h of 0.008 mg/L and it reached concentrations of 0.628 mg L^{-1} after 25 h operation. A consequence of the instability of CuHCF during long-term cycling test is the oxidation and reduction of copper bound to the nitrogen atom (Pothanamkandathil et al., 2020). The poor stability of CuHCF coating was further affected by the high flux rate of the stream over long-term cycling analysis. Takahashi et al. (2015) observed that the crystallite size of CuHCF aggregates decreased from 22 nm to 11 nm when using a micro-mixer and increasing the flow rate of a synthetic stream containing Cs^+ to 100 mL min^{-1}. Thus, the reduced crystallite size of CuHCF in our study led to a weak bonding between the binding material and the small-sized CuHCF material, which, in turn, caused CuHCF material to loose electrical contact with the electrode matrix over long-term cycling.

Although the results so far demonstrated the feasibility of this CuHCF approach for ammonia recovery, further studies are clearly needed to improve the stability of the electrodes. A conformal layer could be introduced to prevent the dissolution of CuHCF, for example, by adding metal oxides such as Al_2O_3 and TiO_2, amines such as ethylenediamine and insoluble transition metal sulfides such as Cu_2S and ZnS to the aqueous solution containing synthesized CuHCF (Wessells and Huggins, 2017). Moreover, the dissolution of cations from MHCFs could be reduced by structural modifications as well. For example, the highly crystallized core-shell structured cobalt/nickel hexacyanoferrate can be coated by the NiHCF to suppress lattice distortion and side reactions (Yin et al., 2019). It was found that benefitting from limited charge/discharge depth, the inactive Ni^{2+} ions introduced to the MHCF framework can minimize the atom distortions in an inert atmosphere of argon, thereby improving the electrochemical stability of coin-sized electrodes. Electrodes with long-term stability would enable further investigating insertion and regeneration potentials to improve stability, not necessarily aiming at maximizing insertion/regeneration capacity. Additionally, an optimal binder to accommodate the volume variation of CuHCF during cycling tests still needs to be identified. Other possibilities include a binder synthesized by Song et al. (2014) using a low-cost water soluble poly(acrylic acid) (PAA) and polyvinyl alcohol (PVA) precursors. This binder was found to enhance bonding between Si and the binding material, which accommodated the large volume change of the silicon anode during adsorption, resulting in excellent cycling stability (1663 mAh g^{-1} after 80 h).

4. Conclusions

- CuHCF coated electrodes were shown to separate and recover NH_4^+ from a real industrial wastewater at 0.3 V (vs. Ag/AgCl) without interference from anions and organics present.
- At a regeneration potential of 1.1 V (Vs. Ag/AgCl), 88.9 ± 0.4 % of inserted NH_4^+ was released back to the solution.
- Cl^- ions negatively affected the stability of the CuHCF coated electrodes due to Cl_2 production at the carbon anode caused by the high counter potential.
- A minimal NH_4^+ concentration of 71.57 ± 0.12 mg L^{-1} was achieved after 20 cycles of NH_4^+ removal on the real stream, which corresponded to the highest NH_4^+ removal efficiency of 92.9 ± 0.01 %.
- CV and CA analyses showed that the CuHCF electrodes tested here had a poor stability over time. A conductive and resilient binder is needed for the transformable structure of the CuHCF framework and a low-temperature cure.
- Separation of NH_4^+ from wastewater containing organics by CuHCF coated electrodes under constant potential appears to be a promising technology for NH_4^+ removal and recovery and should be further investigated for application in the treatment of complex wastewaters containing high concentrations of ammonia.

Declaration of Competing Interest

The author declares no conflict of interest.

Acknowledgement

Rui Gao gratefully acknowledges support from the Flemish SIM MaRes programme, under grant agreement no. 150626 (Get-A-Met project). Rui Gao and Korneel Rabaey are further supported by the Ghent University Bijzonder Onderzoeksfonds via GOA grant BOF2019/GOA/026/L. All authors are supported by FWO under grant agreement 3G0I188W. The authors thank Erika Fiset, Elien Wyallaert, Ilse Delaere and Davy Deduytsche for the electrochemical, SEM-EDX, optical-microscopy and XRD analyses.

Supplementary materials

Supplementary material associated with this article can be found, in the online version, at doi:10.1016/j.watres.2020.116532.

References

Bhandari, V., Sorokhaibam, L.G., Ranade, V., 2016. Industrial wastewater treatment for fertilizer industry—a case study. Desalin. Water Treat. 57, 1–11.
Champagne, B., Kirtman, B., 2001. Handbook of advanced electronic and photonic materials and devices. Nonlinear Opt. Mater. 9, 63.
Eekert van, M., Weijma, J., Verdoes, N., de Buisonje, F., Reitsma, B., van den Bulk, J., 2012. Explorative Research on Innovative Nitrogen Recovery. Stichting Toegepast Onderzoek Waterbeheer.
Ghica, M.E., Carvalho, R.C., Amine, A., Brett, C.M.A., 2013. Glucose oxidase enzyme inhibition sensors for heavy metals at carbon film electrodes modified with cobalt or copper hexacyanoferrate. Sens. Actuators B 178, 270–278.
Jiang, Y., Minami, K., Sakurai, K., Takahashi, A., Parajuli, D., Lei, Z., Zhang, Z., Kawamoto, T., 2018. High-capacity and selective ammonium removal from water using sodium cobalt hexacyanoferrate. RSC Adv. 8 (60), 34573–34581.
Kim, J.Y., Cho, N.S., Cho, S., Kim, K., Cheon, S., Kim, K., Kang, S.-Y., Cho, S.M., Lee, J.-I., Oh, J.-Y., 2018a. Graphene electrode enabling electrochromic approaches for daylight-dimming applications. Sci. Rep. 8 (1), 2045–2322.
Kim, T., Gorski, C.A., Logan, B.E., 2018b. Ammonium removal from domestic wastewater using selective battery electrodes. Environ. Sci. Technol. Lett. 5 (9), 578–583.
Klika, Z., Kraus, L., Vopálka, D., 2007. Cesium uptake from aqueous solutions by bentonite: a comparison of multicomponent sorption with ion-exchange models. Langmuir 23 (3), 1227–1233.
Krishnaswamy, S., Nazir, S.M., Srikanth, P.V.K., Ponnani, K., 2012. Process Condensate Stripper Performance in Ammonia Plants. Nitrogen+Syngas.
Li, J.-T., Wu, Z.-Y., Lu, Y.-Q., Zhou, Y., Huang, Q.-S., Huang, L., Sun, S.-G., 2017. Water soluble binder, an electrochemical performance booster for electrode materials with high energy density. Adv. Energy Mater. 7 (24), 1701185.
Mimura, H., Kimura, M., Akiba, K., Onodera, Y., 1999. Selective removal of cesium from sodium nitrate solutions by potassium nickel hexacyanoferrate-loaded chabazites. Sep. Sci. Technol. 34 (1), 17–28.
Nightingale Jr., E., 1959. Phenomenological theory of ion solvation. Effective radii of hydrated ions. J. Phys. Chem. 63 (9), 1381–1387.
Parajuli, D., 2016. Prospective application of copper hexacyanoferrate for capturing dissolved ammonia. Ind. Eng. Chem. Res. 55 (23), 6708–6715.
Parajuli, D., Takahashi, A., Noguchi, H., Kitajima, A., Tanaka, H., Takasaki, M., Yoshino, K., Kawamoto, T., 2016. Comparative study of the factors associated with the application of metal hexacyanoferrates for environmental Cs decontamination. Chem. Eng. J. 283, 1322–1328.
Pasta, M., Wang, R.Y., Ruffo, R., Qiao, R., Lee, H.-W., Shyam, B., Guo, M., Wang, Y., Wray, L.A., Yang, W., 2016. Manganese–cobalt hexacyanoferrate cathodes for sodium-ion batteries. J. Mater. Chem. A 4 (11), 4211–4223.
Pasta, M., Wessells, C.D., Huggins, R.A., Cui, Y., 2012. A high-rate and long cycle life aqueous electrolyte battery for grid-scale energy storage. Nat. Commun. 3 (1), 1149.
Pothanamkandathil, V., Fortunato, J., Gorski, C.A., 2020. Electrochemical desalination using intercalating electrode materials: a comparison of energy demands. Environ. Sci. Technol. 54 (6), 3653–3662.
Qin, M., Liu, Y., Luo, S., Qiao, R., He, Z., 2017. Integrated experimental and modeling evaluation of energy consumption for ammonia recovery in bioelectrochemical systems. Chem. Eng. J. 327, 924–931.
Sharma, S.K., Sanghi, R., 2012. Wastewater Reuse and Management. Springer, Netherlands.
Shi, Y., Zhou, X., Yu, G., 2017. Material and structural design of novel binder systems for high-energy, high-power lithium-ion batteries. Acc. Chem. Res. 50 (11), 2642–2652.
Smith, C., Hill, A.K., Torrente-Murciano, L., 2020. Current and future role of Haber–Bosch ammonia in a carbon-free energy landscape. Energy Environ. Sci. 13 (2), 331–344.
Son, M., Aronson, B.L., Yang, W., Gorski, C.A., Logan, B.E., 2020. Recovery of Ammonium and Phosphate Using Battery Deionization in a Background Electrolyte. Environmental Science: Water Research & Technology.
Song, J., Zhou, M., Yi, R., Xu, T., Gordin, M.L., Tang, D., Yu, Z., Regula, M., Wang, D., 2014. Interpenetrated gel polymer binder for high-performance silicon anodes in lithium-ion batteries. Adv. Funct. Mater. 24 (37), 5904–5910.
Takahashi, A., Minami, N., Tanaka, H., Sue, K., Minami, K., Parajuli, D., Lee, K.-M., Ohkoshi, S.-i., Kurihara, M., Kawamoto, T., 2015. Efficient synthesis of size–controlled open-framework nanoparticles fabricated with a micro-mixer: route to the improvement of Cs adsorption performance. Green Chem. 17 (8), 4228–4233.
Valsala, T.P., Joseph, A., Shah, J.G., Raj, K., Venugopal, V., 2009. Synthesis and characterization of cobalt ferrocyanides loaded on organic anion exchanger. J. Nucl. Mater. 384 (2), 146–152.
Wang, R.Y., Shyam, B., Stone, K.H., Weker, J.N., Pasta, M., Lee, H.W., Toney, M.F., Cui, Y., 2015. Reversible multivalent (monovalent, divalent, trivalent) ion insertion in open framework materials. Adv. Energy Mater. 5 (12), 1401869.
Wang, W., Gang, Y., Hu, Z., Yan, Z., Li, W., Li, Y., Gu, Q.-F., Wang, Z., Chou, S.-L., Liu, H.-K., Dou, S.-X., 2020. Reversible structural evolution of sodium-rich rhombohedral Prussian blue for sodium-ion batteries. Nat. Commun. 11 (1) 980-980.
Wang, Z., Dupre, N., Gaillot, A.-C., Lestriez, B., Martin, J.-F., Daniel, L., Patoux, S., Guyomard, D., 2012. CMC as a binder in LiNi0. 4Mn1. 6O4 5 V cathodes and their electrochemical performance for Li-ion batteries. Electrochim. Acta 62, 77–83.
Wessells, C.D. and Huggins, R.A. (2017) Stabilization of battery electrodes using polymer coatings, U.S.Patent 9,853,318.
Wessells, C.D., Huggins, R.A., Cui, Y., 2011. Copper hexacyanoferrate battery electrodes with long cycle life and high power. Nat. Commun. 2 (1), 550.
Yeh, J.-W., Chang, S.-Y., Hong, Y.-D., Chen, S.-K., Lin, S.-J., 2007. Anomalous decrease in X-ray diffraction intensities of Cu–Ni–Al–Co–Cr–Fe–Si alloy systems with multi-principal elements. Mater. Chem. Phys. 103 (1), 41–46.
Yin, J., Shen, Y., Li, C., Fan, C., Sun, S., Liu, Y., Peng, J., Qing, L., Han, J., 2019. In situ self-assembly of core–shell multimetal Prussian blue analogues for high-performance sodium-ion batteries. ChemSusChem 12 (21), 4786–4790.
Zhang, Y., Sun, X., Zhu, L., Shen, H., Jia, N., 2011. Electrochemical sensing based on graphene oxide/Prussian blue hybrid film modified electrode. Electrochim. Acta 56 (3), 1239–1245.
Zöllig, H., Remmele, A., Morgenroth, E., Udert, K.M., 2017. Removal rates and energy demand of the electrochemical oxidation of ammonia and organic substances in real stored urine. Environ. Sci. 3 (3), 480–491.